Electronic Supplementary Material (ESI) for Nanoscale.
This journal is © The Royal Society of Chemistry 2019

Broad-band high-gain room temperature photodetector using semiconductor–metal nanofloret hybrids with wide plasmonic response

Amir Ziv[a], Avra Tzaguy[b], Zhiyuan Sun[c] ,Shira Yochelis[a], Emmanuel Stratakis[d] George Kenanakis[d], George C. Schatz[f], Lincoln J. Lauhon[c], David N. Seidman[c,e], Yossi Paltiel[a] and Roie Yerushalmi[b*]*

[a]*Department of Applied Physics, the Hebrew University, Jerusalem, Edmond J. Safra Campus, Givat Ram, Jerusalem, 91904, Israel*

[b]*Institute of Chemistry and the Center for Nanoscience and Nanotechnology, the Hebrew University of Jerusalem, Edmond J. Safra Campus, Givat Ram, Jerusalem, 91904, Israel*

[c]*Department of Materials Science and Engineering, Northwestern University, 2220 Campus Drive, Evanston, 60208-3108, USA*

[d]*Institute of Electronic Structure and Laser (IESL), Foundation for Research & Technology-Hellas (FORTH), N. Plastira 100, GR-70013, Heraklion, Crete, Greece.*

[e]*Northwestern University Center for Atom-Probe Tomography (NUCAPT), 2220 Campus Drive, Evanston, 60208-3108, USA*

[f] *Department of Chemistry, Northwestern University, Evanston, 60208-3113, USA*

Content of Supporting Information:

1. Measurement Setup Description:

The prepared samples with NF/NW junctions were bonded using a wire bonder. All electronic measurements were performed inside a Faraday cage. The device was connected utilizing BNC connections to a Keithley 6487 Picoammeter/Voltage Source. Measurements were performed at a sampling rate of 20 Hz (50 ms between each current measurement).

The photoresponse was obtained by illuminating the sample with different CW laser sources, below are the measured powers of the lasers:

Wavelength [nm]	Area [cm^2]	Measured Power [mW]	Power per unit area [W/cm^2]
405	1.57	75.4	0.048
532	0.00785	98.8	12.58
660	0.01767	113.6	6.06
785	0.03141	72.7	2.314
1064	0.00785	16.25	2.070
1550	0.377	131	0.347
1850	0.25	110	0.44

2. D* and g Calculations:

The specific detectivity, D* was calculated using the following equation:

$$1 \quad D^* = R \cdot \frac{\sqrt{A\Delta f}}{i_{noise}}$$

Where A is the detector's effective area, Δf is the bandwidth and i_{noise} is the current's noise. The letter R is the responsivity and is calculated employing the following equation:

$$2 \quad R = \frac{i_{photo}}{\eta \cdot P \cdot A}$$

Where i_{photo} is the photocurrent, η is the internal quantum efficiency, P is the photon irradiance and A is the effective illuminated area. It is important to note that the quantum efficiency that is taken into account is the internal quantum efficiency, that is, the ratio between the collected charge carriers and the photons absorbed by the sample. Since we are interested in the photodetection of the plasmon structure, or in other words, we are not aiming to improve the external quantum efficiency, but rather to improve and enhance the detectivity of each absorbed photon. The quantum efficiency of a monolayer of nanowires is estimated to be about 0.1

The effective detector area was calculated assuming five NF structures in each device (with an error of two NF). While for each NW the effective area was estimated to be 60 nm in width (twice the radius) and 300 nm in length – the length of the floret.

The photo current was calculated by taking a histogram of periods of dark and light currents, performing a Gaussian fit and taking the peak position as the current value, and the full-width-half-

maximum (FWHM) as the error. For the current's noise, a Fourier transform, followed by a Gaussian fit to a histogram was performed. These calculations are demonstrated below:

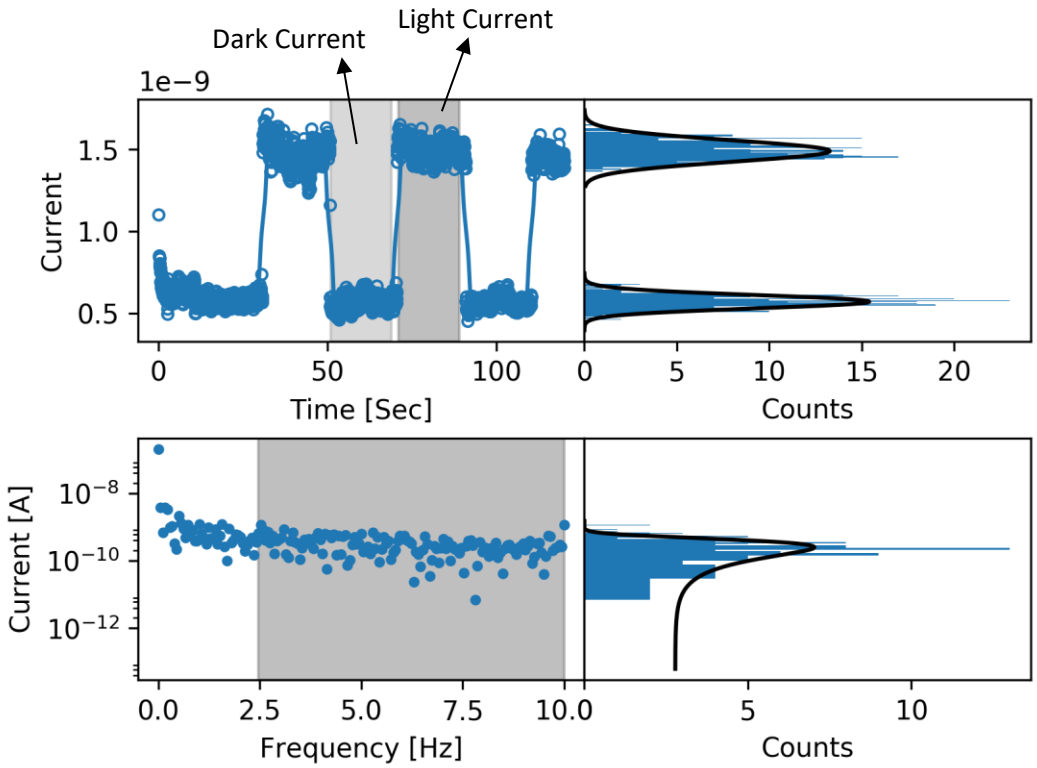

Figure S1. Top: the dark current period is highlighted in grey and the light current is highlighted in a darker grey color. To the right, a histogram and a Gaussian fit are shown. Bottom: Fourier transform of the dark current, in grey is the part were the histogram a fit was performed.

The photoelectric gain was calculated using the following equation:

$$g = \frac{(i_{photo}/e)}{((\eta \cdot P \cdot A \cdot \lambda)/(h \cdot c))} \quad (3)$$

Where i_{photo} is the calculated photocurrent described earlier, e is the charge of an electron, η is the internal quantum efficiency, P is the photon irradiance, A is the effective illuminated area, λ is photon's wavelength, h is the Planck's constant and c is the speed of light.

Investigation of the dark current behavior showed differences between the NW and the NF devices. In most cases, the noise distribution in the NW devices is gaussian, whereas the noise distribution in the NF device show several peaks, which we ascribe to trapping/detrapping events in traps close to the gold tip. Two examples for such dark current are presented below:

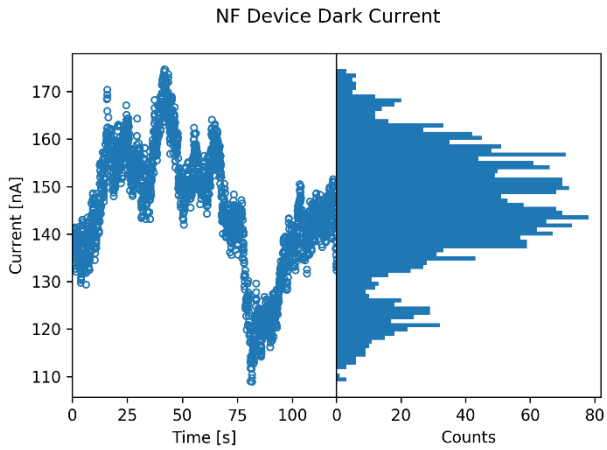

Figure S2. Dark current of a NF device.

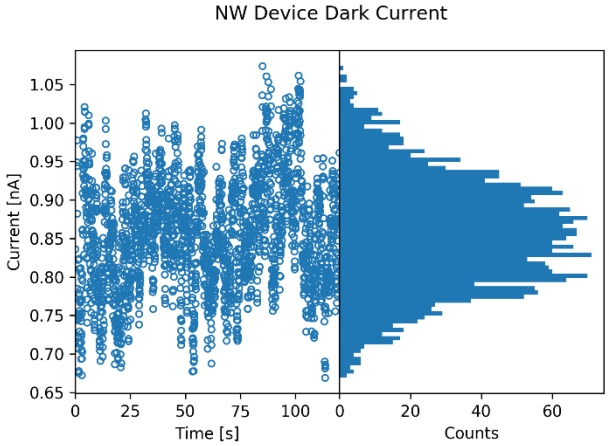

Figure S3. Dark current of a NW device.

3. Current-Voltage Characteristics:

Two examples of the current-voltage characteristics in one NW and one NF devices:

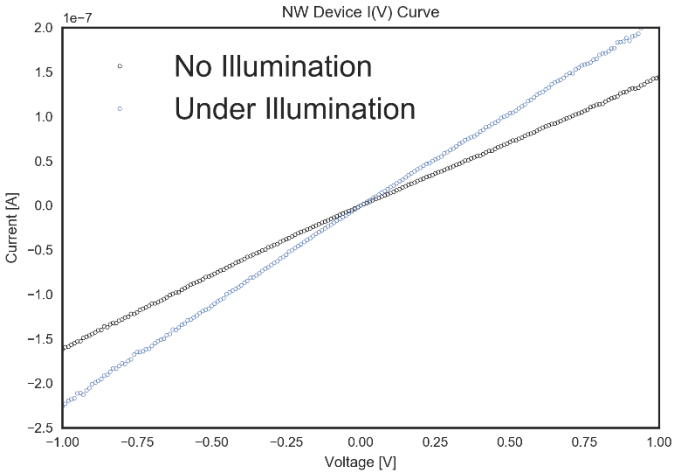

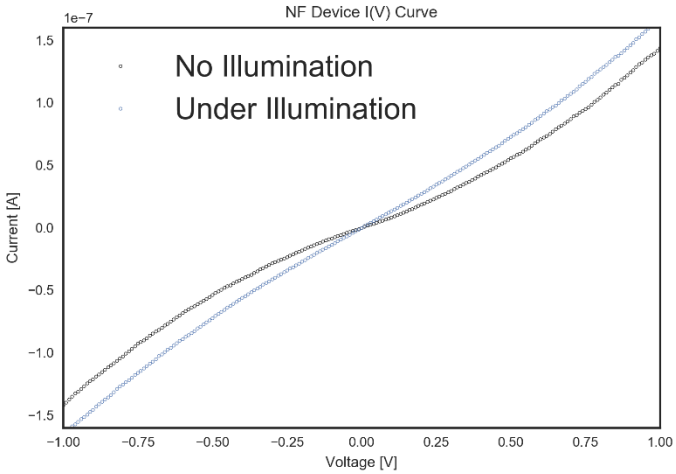

Figure S4. Current voltage characteristics.

4. Current Photoresponse Time Dependence:

Presented below are measurements of the current as a function of time under illumination, for several wavelengths:

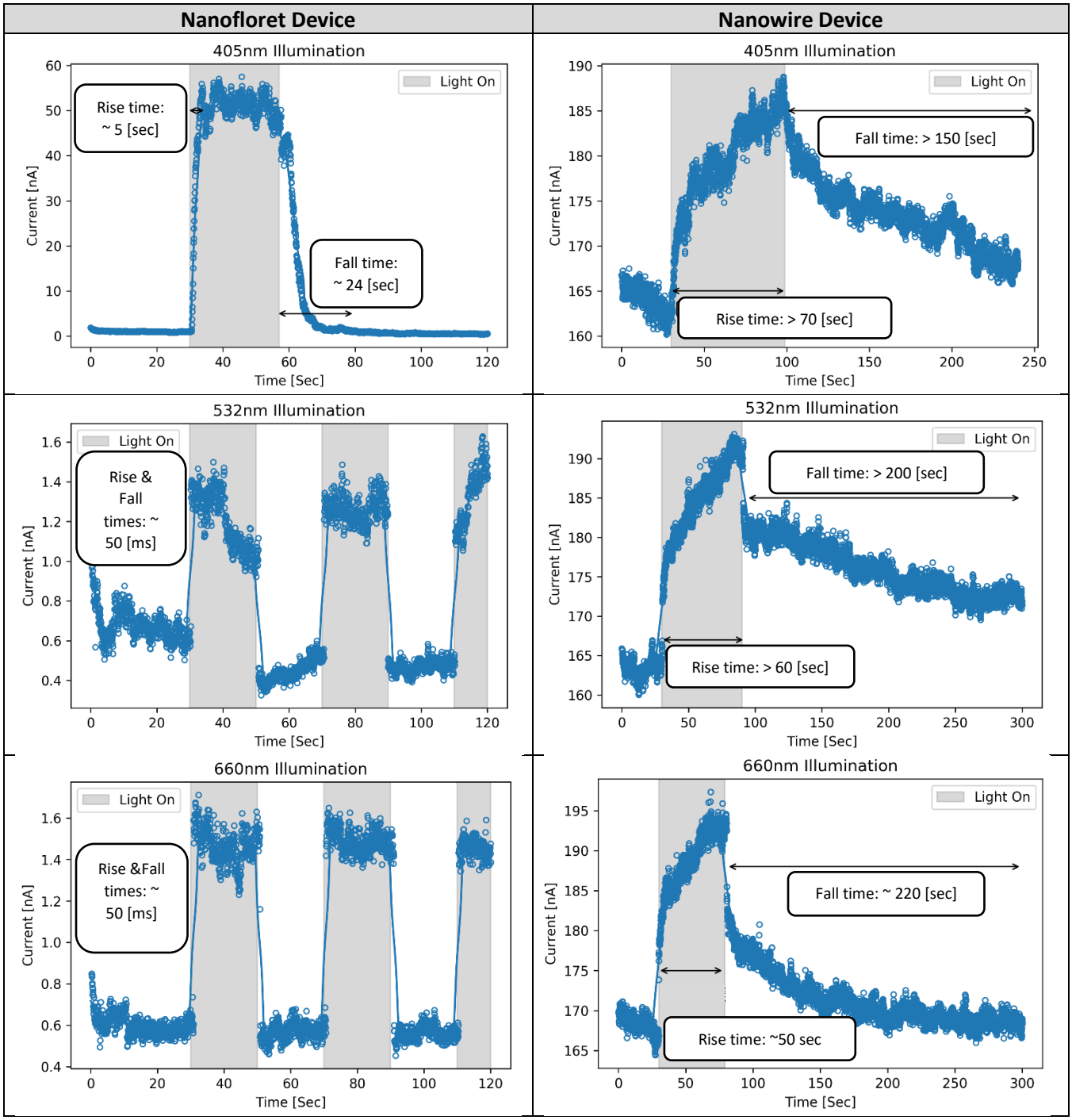

Figure S5

For both types of devices, the rise and fall times under 405 nm illumination are longer. Whereas for the NF device there is an improvement compared to the NWs, however it is still slower compared to other wavelengths.

5. Comparison Between Different Junctions:

In figure S3 there are comparisons between three different NF devices which demonstrates the ability to tune the device resonance according to the different morphologies of each specific nanofloret structure.

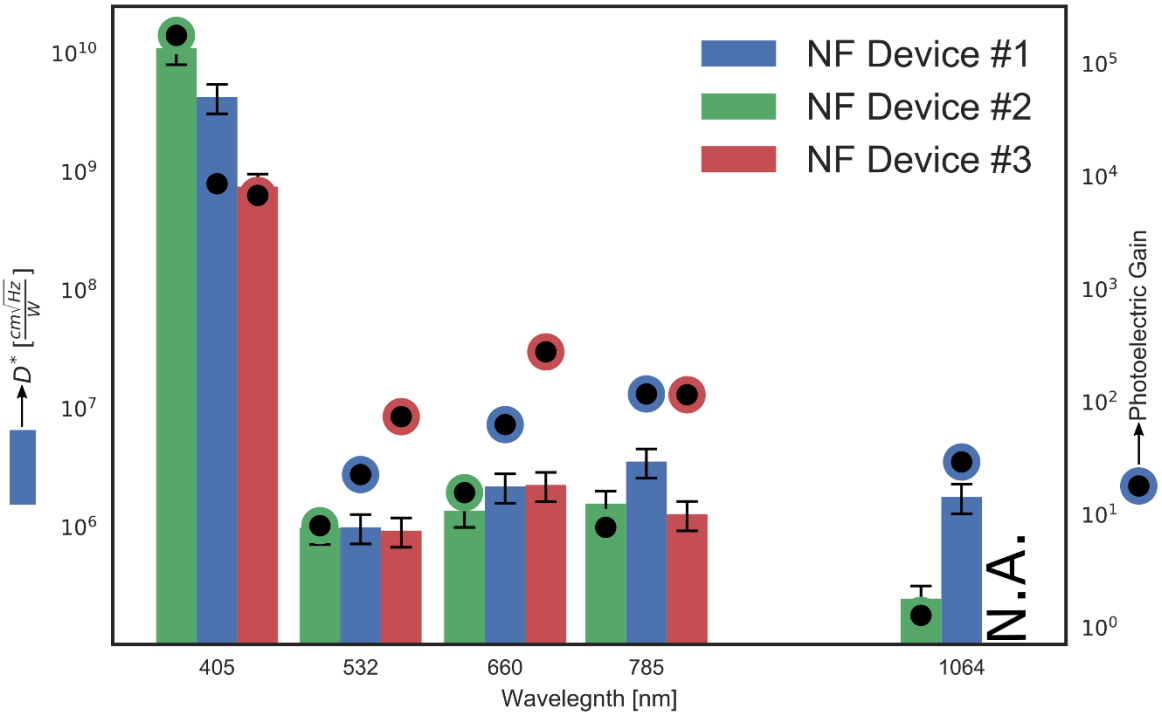

Figure S6

6. NF Devices with Coupling to surface states

Below are examples to the photoresponse of NF devices where the photoresponse rate was slower compared to other NF devices, but still much faster compared to unmodified NW devices. We attribute this difference to coupling between the localized plasmon to surface states, which increase the photoresponse, with the prices of slower response time.

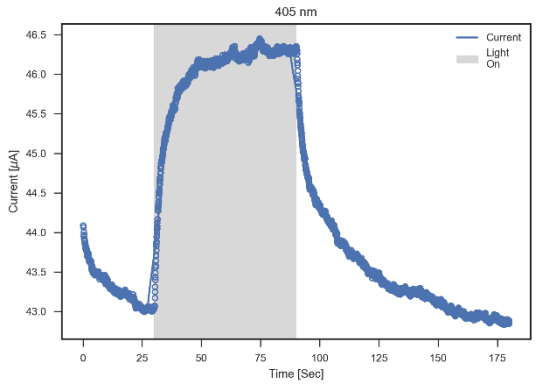
405 nm
Current
Light On
Current [μA]
Time [Sec]

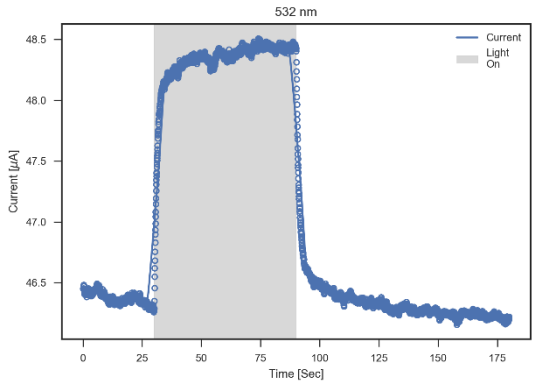
532 nm
Current
Light On
Current [μA]
Time [Sec]

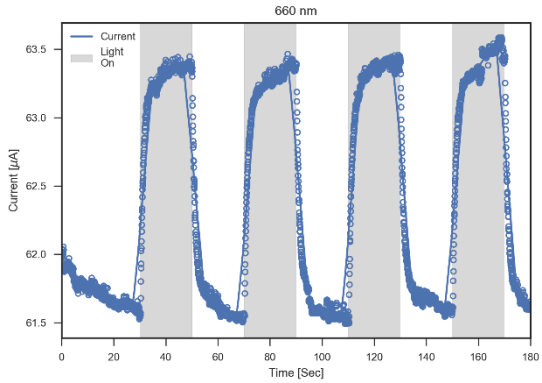
660 nm
Current
Light On
Current [μA]
Time [Sec]

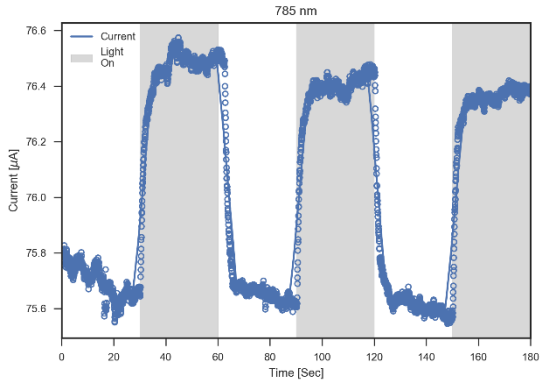
785 nm
Current
Light On
Current [μA]
Time [Sec]

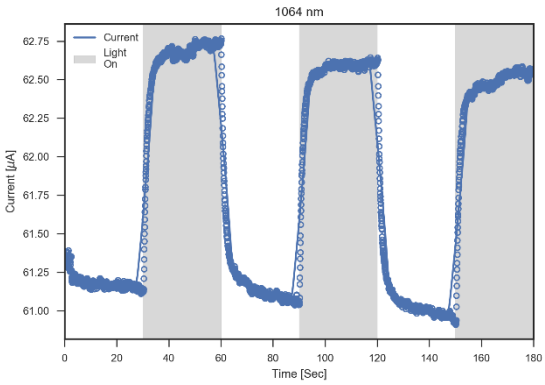
1064 nm
Current
Light On
Current [μA]
Time [Sec]

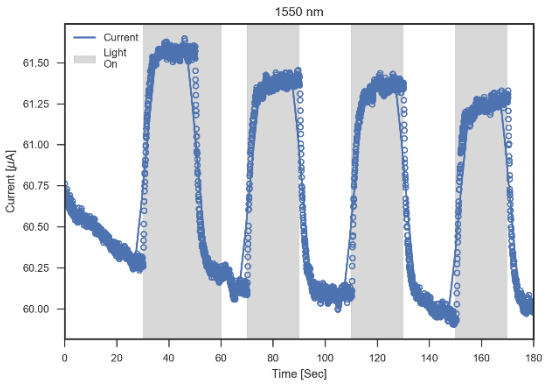
1550 nm
Current
Light On
Current [μA]
Time [Sec]

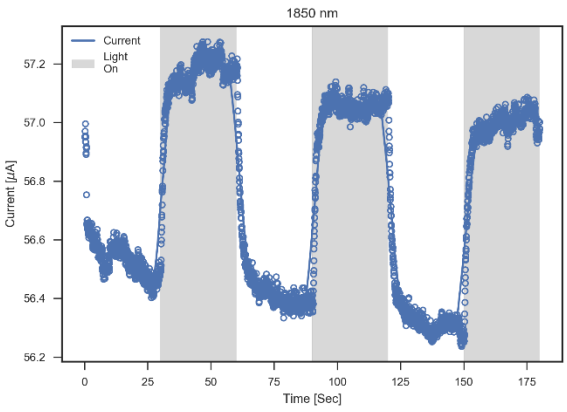
1850 nm
Current
Light On
Current [μA]
Time [Sec]

7. Simulation Scheme Description

Electromagnetic simulations were performed using a commercial three-dimensional full-wave solver (CST Microwave Studio, Computer Simulation Technology GmbH, Darmstadt, Germany) based on the finite integration technique (FIT), using the time domain solver in the wavelength range 300 to 2500 nm. First, a model for the NF structure was created by placing gold nanoparticles around the edge of a Ge cylinder, separated by a GeO_2 layer (the dielectric functions utilized are described below). The radii of the nanoparticles (r), their edge-to-edge separation (d) and length (L) of the floret structure were all controlled. An example of the structure is displayed in figure S4.

The system was simulated by illuminating it with CW illumination. Each simulation was performed utilizing two polarizations, parallel and perpendicular to the NF structure (see section 6 for further details). A far field monitor was used, which calculated the electromagnetic far field in all possible directions, and the radar cross section (RCS) and absorption cross section (ACS) were calculated.

The RCS is defined employing the following expressions:

$$4 \quad RCS = 4\pi \frac{Power\ scattered\ per\ unit\ solid\ angle}{irradiance\ due\ to\ incoming\ plane\ wave}$$

And the definition for the ACS is similar.

The total extinction cross section is simply the sum of ACS and RCS.

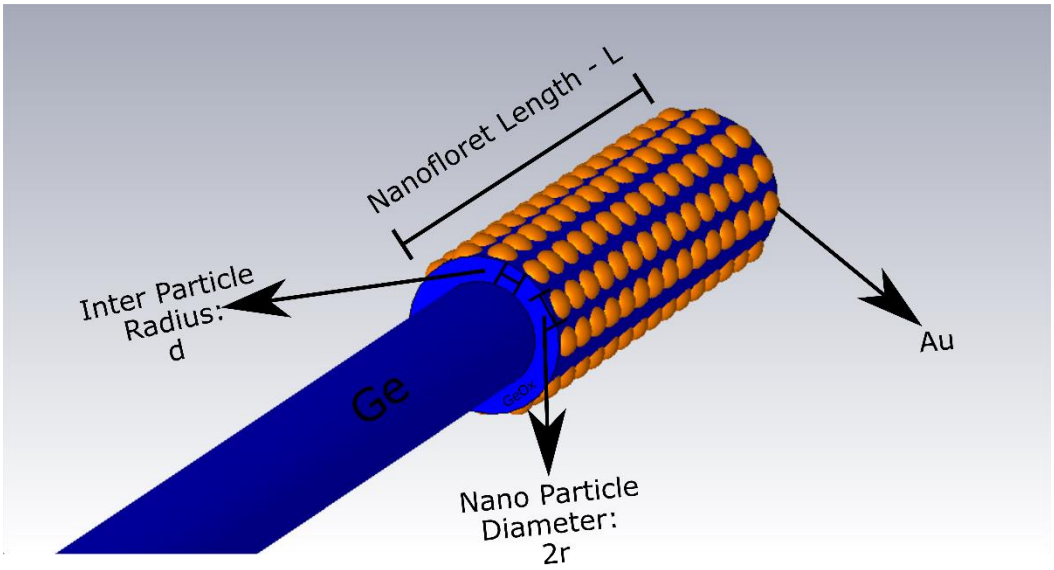

Figure S7

Au	Johnson and Christy 1972[1]
Ge	Aspnes and Studna 1983[2]
GeO2	Fleming 1984: Fused germania[3]
Plane wave:	Far field monitor:

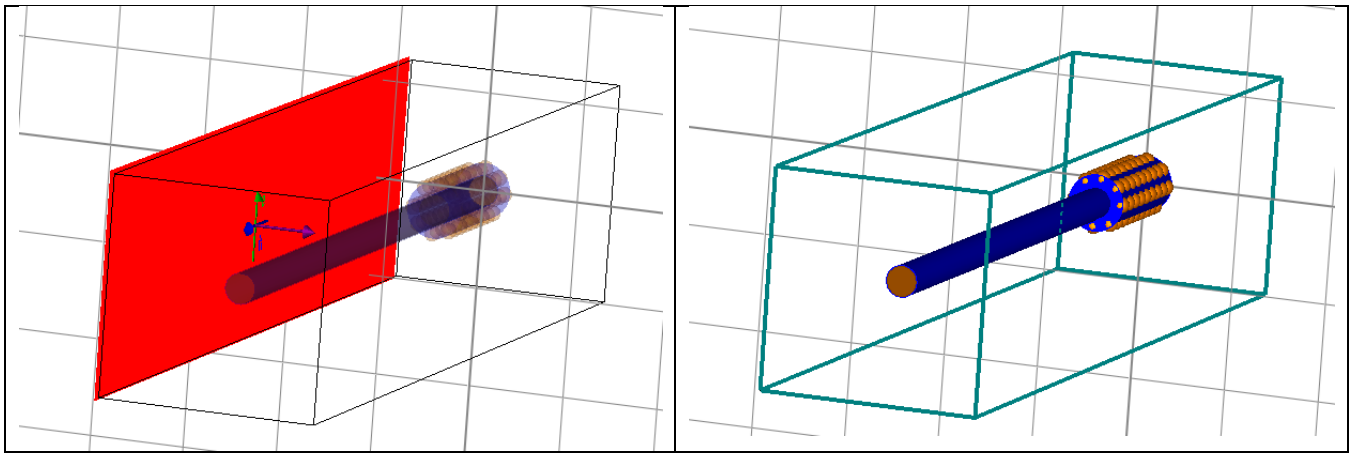

8. Additional Simulation Results

Each simulation was performed for two polarizations, parallel or perpendicular to the NF structure. Below is a comparison of the polarization for the NF structure:

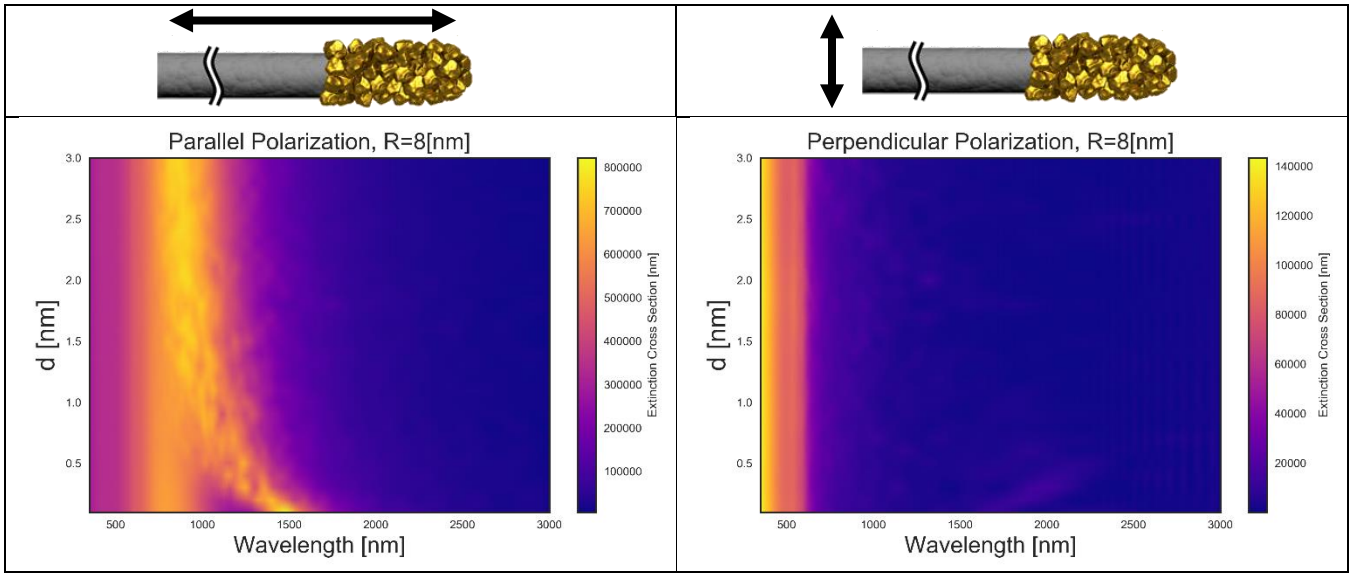

Figure S8

It is apparent that the collective plasmonic resonance occurs only with the parallel polarization, and therefore the coupling between the individual gold NPs leads to plasmon modes that are delocalized along the NF's long axis but not the curved short axis. To understand this better, the same simulation was performed on the shell only, that is, without the semiconducting NW. Below are the results for the shell-only structure:

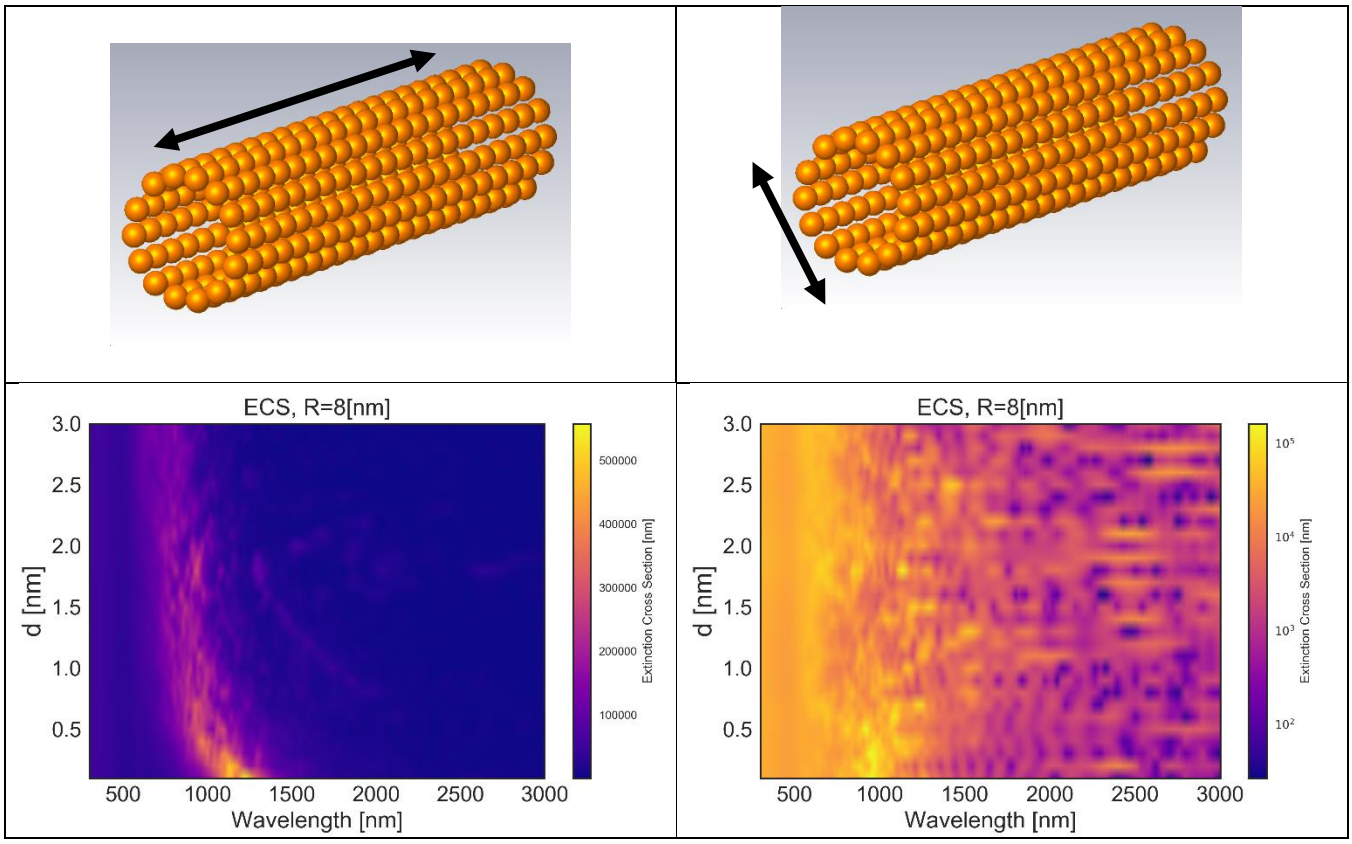

Figure S9

It is clear that for the parallel polarization case, the resonance is blue shifted but is otherwise similar to Fig. S5. This is also true for the perpendicular polarization case, where the resonance occurs at around 600 nm as a continuous line, and with reduced intensity for very close distances (notice that the graph utilizes a log scale).

Next, the simulation was repeated with a structure consisting of a planar array whose dimensions correspond to a flattened NF shell. The results are below:

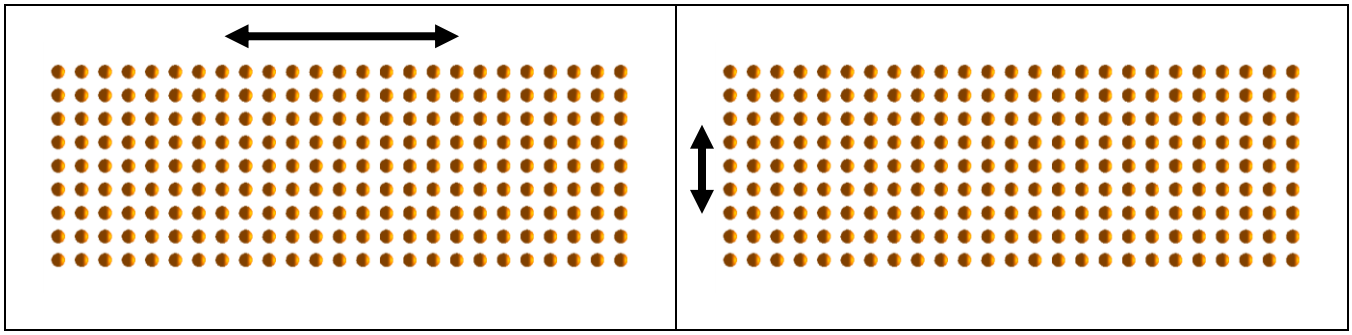

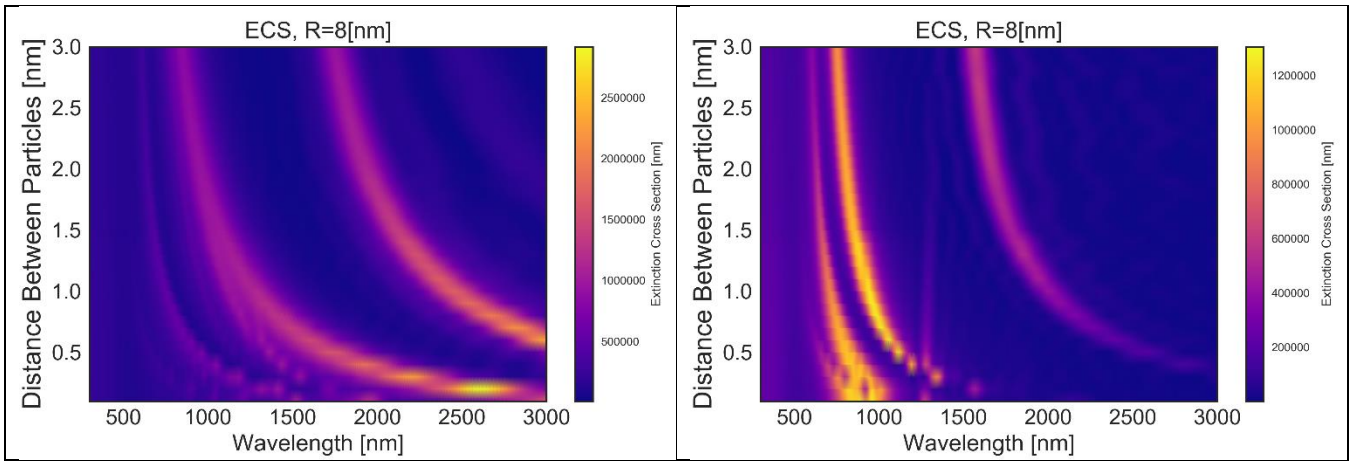

Figure S10

Here, the results are determined by lattice plasmon effects, where the calculated discrete modes are associated with band edges in the dispersion behavior. This suggests that peaks in the NF gold shell results involve extinction in-between the band edges, hence the broader spectral response.

Finally, a model of continuous smoothed gold nanotip was simulated. Below are examples of sweeping both the radius of the NF and the lengths of the gold nanoshell cap (both with parallel polarization):

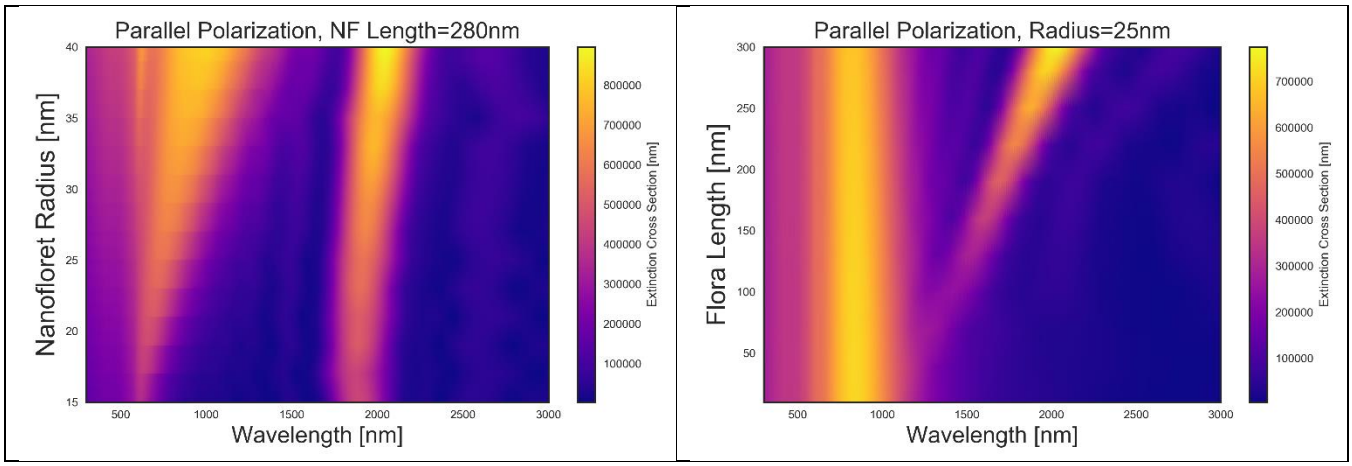

Figure S11

It appears that changing the radius affects response in the near infrared regime (NIR), whereas the length (L) changes the SWIR regime. These resonances are the perpendicular and parallel modes of the gold tip, such that increasing the radius or length leads to red shifting and broadening due to radiative depolarization and damping effects.

References:

1. P. B. Johnson and R. W. Christy. Optical constants of the noble metals, *Phys. Rev. B* **6**, 4370-4379 (1972)
2. D.E. Aspnes and A. A. Studna. Dielectric functions and optical parameters of Si, Ge, GaP, GaAs, GaSb, InP, InAs, and InSb from 1.5 to 6.0 eV, *Phys. Rev. B* **27**, 985-1009 (1983)
3. J. W. Fleming. Dispersion in GeO_2-SiO_2 glasses, *Appl. Opt.* **23**, 4486-4493 (1984)